New Journal of Physics
The open-access journal for physics

Hard x-ray photoelectron spectroscopy of oxide hybrid and heterostructures: a new method for the study of buried interfaces

R Claessen[1,3], M Sing[1], M Paul[1], G Berner[1], A Wetscherek[1], A Müller[1] and W Drube[2]

[1] Experimentelle Physik 4, Am Hubland, Universität Würzburg, D-97074 Würzburg, Germany
[2] Deutsches Elektronen-Synchrotron (DESY), Notkestrasse 85, D-22607 Hamburg, Germany
E-mail: claessen@physik.uni-wuerzburg.de

New Journal of Physics **11** (2009) 125007 (16pp)
Received 15 June 2009
Published 11 December 2009
Online at http://www.njp.org/
doi:10.1088/1367-2630/11/12/125007

Abstract. Hard x-ray photoelectron spectroscopy (HAXPES) is a new variant of the well-established photoemission technique, which extends its range to much higher photoelectron energies up to 10 keV and thus to enhanced probing depths of the order of 10 nm and beyond. This not only facilitates direct access to the intrinsic *bulk* electronic structure of solids, but also allows extended depth profiling and the study of buried interfaces not possible by conventional photoemission. Here, we present two HAXPES case studies on transition metal hybrid and heterostructures demonstrating the potential of the method. We also discuss a new HAXPES setup at the high-brilliance hard x-ray synchrotron radiation source PETRA III at DESY (Hamburg) currently under construction.

[3] Author to whom any correspondence should be addressed.

Contents

1. Introduction

Ever since the Nobel prize-awarded work by Kai Siegbahn, photoelectron spectroscopy (PES) has evolved into a well-established and powerful method for the investigation of atoms, molecules and solids. In particular for the latter, PES allows a detailed elucidation of the microscopic electronic structure, as it provides direct access to the density of states, the band structure and the Fermi surface of solids [1]–[3]. PES on the core levels can yield additional information on chemical composition and bonding as well as on local structure. Unfortunately, these applications have remained limited largely to the study of *surfaces* due to the rather small escape depth of the photoelectrons.

The photon radiation required for excitation of the photoelectrons has to be of sufficient energy to overcome the materials work function, and at the same time to be of high enough intensity to allow for a decent signal-to-noise ratio in the photoelectron current as well as for reasonable monochromatization. Using various types of laboratory light sources as well as synchrotron radiation these requirements are well met in the spectral range from the vacuum ultraviolet (VUV) up to the soft x-ray regime, resulting in kinetic energies of the photoelectrons of typically ∼15–1500 eV. Under such conditions, the inelastic mean free path of the photoelectrons is limited to a few nanometers or even below, depending on their kinetic energy but largely irrespective of the actual material ('universal curve') [1]. This restricts the information obtained by PES to a very thin layer of atomic dimensions at the solid–vacuum interface, rendering it a truly surface-sensitive technique. Indeed, PES has been (and still is) an important methodical cornerstone of modern surface science.

However, when interested in the genuine *bulk* electronic structure of solids, the small information depth can become a major obstacle. The breaking of lattice translation symmetry at the surface often leads to structural relaxations or reconstructions with subsequent effects on electronic states at and near the surface. In these cases, the electronic structure probed by conventional PES can strongly deviate from the bulk, except for special situations where the surface termination represents only a minor disturbance, e.g. in quasi-two-dimensional (2D) or 1D materials with van der Waals gaps.

With the advent of high brilliance synchrotron-based light sources in the hard x-ray regime (up to ∼10 keV and beyond) and parallel development of suitable high-energy electron energy analyzers, these shortcomings have recently been overcome [4]. According to the universal curve, hard x-ray PES (HAXPES) allows probing depths of up to 10 nm, in some cases even 20 nm have been demonstrated. Bearing in mind that surface relaxations typically decay on a length scale of a lattice constant and that the unit cell dimension of even complex materials rarely exceed ∼1 nm, HAXPES has the potential to access the intrinsic electronic structure of the bulk. Over the past 5–6 years intense activities in Japan, but also in Europe, have pushed forward the development of the technique and produced numerous examples of its power. A very comprehensive and up-to-date overview of the field, including instrumental and technical aspects of HAXPES as well as various examples of applications from basic science to industrial research, has very recently been given by Kobayashi [5].

Beyond the access to the bulk, the enhanced probing depth of HAXPES also allows for extended *depth profiling* of ultrathin films and, in particular, for the study of the *buried interface* between overlayer and substrate, i.e. between different materials. A case in point is heterostructures consisting of transition metal oxides (TMO). Due to the complex interplay between various microscopic degrees of freedom (charge, spin, orbital and lattice) in TMOs, already the pure materials display a plethora of highly interesting many-body effects and cooperative phenomena, ranging from correlation-induced metal–insulator transitions to high-temperature superconductivity (see e.g. [6]). Due to the enormous progress in molecular beam epitaxy (MBE) and pulsed laser deposition (PLD) of complex oxides, it has recently become possible to grow epitaxial films and oxide heterostructures of unprecedented quality [7]. It turns out that the combination of different oxides can lead to unexpected new phenomena which cannot be anticipated from the properties of each constituent alone. This opens the door for tailoring novel functionalities through the appropriate choice of materials.

In this paper, we will discuss two examples for HAXPES studies of oxide hybrid and heterostructures. The first one concerns depth profiling of hybrid structures made of ultrathin magnetite (Fe_3O_4) films grown on III–V semiconductors, which can be viewed as a prototypical model system for a spin injection electrode in spintronics. In the second example, we study the formation of a 2D electron gas (2DEG) which is formed at the interface between two otherwise insulating TMOs. Both case studies serve to demonstrate the potential and possibilities of HAXPES. Finally, we will give a short description of a new HAXPES set-up presently under construction at the new high-brilliance hard x-ray synchrotron light source PETRA III at DESY (Hamburg), which will aim especially at the study of magnetic systems.

2. Experimental

The HAXPES experiments presented here have been performed at two separate synchrotron beamlines. One is the bending magnet crystal monochromator beamline KMC-1 of BESSY (Berlin) using their high kinetic energy (HIKE) photoemission endstation [8]. The monochromator operates in the $(n, -n)$ double crystal arrangement with constant beam offset. For tuning the photon energy from the soft x-ray regime (1.7 keV) up to the hard x-ray regime (12 keV), four sets of crystals, InSb(111), Si(111), Si(311) and Si(422) are available. The photon flux depends on the chosen set of crystals and is about 10^{11}–10^{12} photons s^{-1}. The photoelectron spectrometer of the HIKE endstation is a Gammadata Scienta R-4000 hemispherical analyzer,

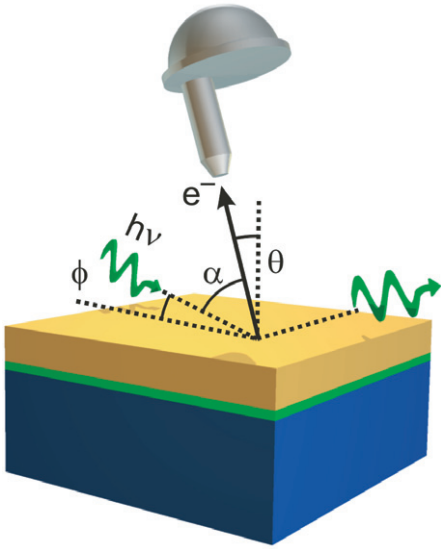

Figure 1. Measurement geometry used for angle-dependent photoemission experiments. ϕ denotes the angle of incidence, α is defined as the angle between incoming beam and spectrometer and θ is the emission angle with respect to the surface normal.

which is optimized for HIKE electrons up to 10 keV. The total energy resolution using the Si(111) crystal for 3 keV photons amounts to 500 meV.

The other experimental site is the BW2 beamline of the DORIS III storage ring at DESY (Hamburg), which employs a high heat-load Si(111) double crystal monochromator. The intrinsic resolution for the used Si(111) crystal pair is $\Delta E/E \approx 1.5 \times 10^{-4}$ with a corresponding energy bandpass of 450 meV at 3000 eV. Due to the wiggler beamline the photon flux at this energy is about 3×10^{12} photons s^{-1}. The focus size on the sample amounts to 0.3 mm (vertical) $\times$ 2 mm (horizontal). The photoelectrons are detected by a SCIENTA SES-200 electron spectrometer optimized for photoemission in the hard x-ray regime [9].

One of the most prominent features of HAXPES is its possibility to perform depth profiling measurements. Due to the inelastic mean free path's dependence on the excitation energy depth profiling is possible by varying the excitation energy at constant photoelectron emission angle. The escape depth as a function of excitation energy basically shows a logarithmic slope in the hard x-ray regime. Therefore, it is possible to tune the information depth without changing the measurement geometry. An inevitable side effect is the non-negligible energy dependence of the photoelectron cross-sections. Alternatively, one can use angle-dependent HAXPES at constant excitation energy. This conventional method of depth profiling is based on the angle-dependence of the effective escape depth $\lambda_{\mathrm{eff}} = \lambda \cos\theta$ of the photoelectrons.

A third method for depth profiling exploits the effective angle-dependence of the *x-ray penetration depth* in grazing incidence geometry, or more precisely: at and near the angle of *total external x-ray reflection*. In this case, one makes use of the excitation of the photoelectrons by an evanescent wave near the sample surface. By changing the incidence angle ϕ around the critical angle ϕ_c, it is possible to tune the x-ray penetration depth (see figure 1).

3. Fe_3O_4 thin films on semiconductor substrates

3.1. Motivation: magnetite for spintronics

In recent years, the ferrimagnetic iron oxide magnetite (Fe_3O_4) has received much attention, because its properties make it a highly interesting material for applications in the currently developing field of spintronics [10]. The basic concept of spintronics consists in the design of integrated circuits, which use the electron spin for storage and processing of information [11]. The spin-transistor proposed by Datta and Das [12] is one example of a spintronic device. A general problem for the development of such devices is the combination of semiconducting materials, that are commonly used in conventional charge-based electronic chips, and room-temperature ferromagnetic materials that are currently employed in storage devices. For example, a key element of the spin transistor is the injection of a spin current into a semiconductor using a highly spin-polarized electrode. Therefore, a key element is to understand the material science of the growth of magnetic materials like oxidic half-metallic ferrimagnets on substrates used in existing semiconductor technology such as Si, GaAs or InAs.

In this context magnetite stands out from other feasible magnetic materials due to the following bulk material characteristics: a very high Curie temperature of 858 K, a predicted spin-polarization of 100% at the Fermi level [13] and a conductivity of $2.5 \times 10^4\ (\Omega\mathrm{m})^{-1}$ at room temperature [14], which matches quite well the value of semiconducting materials. For a film-substrate structure without buffer layer, the latter two features are crucial to facilitate efficient spin-injection into the semiconducting host via an ohmic contact [15].

Hence, there exists a clear need to study the growth behavior and thin film properties of magnetite on semiconducting substrates like GaAs and InAs. Moreover, a detailed knowledge of the actual interface structure and stoichiometry is desirable in order to correlate them with the magnetic and spin transport properties. Interface issues as the occurrence of mixed phases could prevent a successful growth or at least influence material properties in an undesired way, e.g. limit the degree of spin-polarization at near-interface layers or surfaces. To give numbers, the experimentally determined spin-polarization of Fe_3O_4 ranges from -55% [16]–[18] for the free (100) surface to -80% [19] for the free (111) surface.

Experimental reports on the growth of Fe_3O_4 on semiconducting substrates are still scarce [20]–[22]. Moreover, the problem of interface formation (including the occurrence of interface phases and interface reactions) of these hybrid structures is poorly understood [21, 23]. Here, we present HAXPES data that allow us to characterize Fe_3O_4/semiconductor interfaces through identification of all relevant chemical species, their qualitative and quantitative analysis, and correlating interface quality and depth profile with the preparation conditions (see also [24]).

3.2. Sample fabrication and experimental

The InAs substrates were cut from a Zn-(p-)doped wafer and wet-chemical etched prior to loading into the UHV growth chamber. The GaAs substrate consisted of a commercial Si-doped wafer with an MBE grown undoped GaAs buffer layer and an amorphous As cap layer. As an *in situ* treatment the GaAs substrate was decapped by heating, sputtered (Ar^+, energy 0.6 keV) and annealed to 700 K, while the InAs substrate was annealed only to 770 K prior to actual film growth. As we verified by *in situ* x-ray photoelectron spectroscopy (XPS) measurements these substrate treatments result in clean GaAs and InAs without their native oxides. The good

substrate quality was in both cases confirmed by sharp low energy electron diffraction (LEED) patterns.

Fe_3O_4/GaAs(100) was fabricated by pure Fe film growth at room temperature and post-oxidation at 600 K and $p(O_5) = 1 \times 10^{-5}$ mbar for 12 min following the method applied by Lu *et al* [20]. The deposited Fe film thickness was about 60 Å as derived from angle-resolved (conventional) XPS measurements.

Fe_3O_4/InAs(100) samples were grown by reactive oxide MBE, i.e. a simultaneous deposition of Fe arriving from an electron-beam evaporator and O_2 from an appropriate molecular oxygen background pressure. Here, the Fe_3O_4 film thickness was about 60 Å as derived from XPS measurements, as well.

HAXPES experiments were carried out at room temperature and without further surface treatment to avoid a change in chemical composition. The shown spectra have been shifted to correct for charging by setting the O 1s binding energy to 530.1 eV, which is known to be the same in all Fe oxides [25].

3.3. Results

3.3.1. Fe_3O_4/InAs. In the case of InAs, Fe and O_2 were co-deposited onto the substrate (i.e. by reactive oxide MBE) comparable to the procedure in [22]. The lattice mismatch between Fe_3O_4(100) and InAs(100) faces is only -1.6% assuming that one Fe_3O_4 unit cell with lattice constant 8.397 Å grows on two InAs surface unit cells with single lattice constants of 4.27 Å. This corresponds to an in-plane rotation of the Fe_3O_4(100) face against the InAs(100) face by 45°. However, in a PLD growth study [23] other orientations have been proposed as well. The absence of clear LEED patterns of the Fe_3O_4/InAs thin films prepared in our study suggests that the growth result is rather polycrystalline or textured with in-plane random orientation, but not epitaxial.

The Fe oxidation state of the thin film can be derived from the Fe 2p spectra in figure 2(a). The Fe $2p_{3/2}$ and $2p_{1/2}$ main line peak positions are 710.5 and 724.0 eV, respectively, in excellent agreement with literature values for magnetite (e.g. [26]). In addition, the occurrence and intensity of the so-called $2p_{3/2}$ charge-transfer satellites, which appear additionally to the $2p_{3/2}$ main line indicate the oxidation state of different iron oxides. In the case, of Fe_2O_3, the Fe^{3+} charge-transfer satellite should occur at 719 eV, while for divalent FeO, the Fe^{2+} satellite appears at 715.5 eV. For the mixed valence state of Fe_3O_4 ($Fe^{3+} : Fe^{2+} = 2 : 1$), both satellites add up in such a way that the spectral region between the $2p_{3/2}$ and $2p_{1/2}$ main lines becomes smooth and structureless. The Fe 2p spectra in figure 2(a) exhibit this structureless line shape characteristic for magnetite, thus suggesting that the magnetite film is nearly stoichiometric. Moreover, there is no significant difference between spectra taken at different emission angle showing that the oxidation state at different probing depths is essentially the same. We thus conclude that reactive codeposition of Fe and O_2 with suitable Fe/O_2 ratio for each deposition stage yields well-oxidized magnetite even on a problematic substrate such as InAs.

We add that the small feature at 703 eV just next to the Fe $2p_{3/2}$ main line originates from the In $p_{1/2}$ level. As signal from the substrate it is notedly suppressed for larger electron emission angle θ and hence smaller probing depth, as one would expect.

The study of the other substrate core levels As $2p_{3/2}$ (see figure 2(b)) and In $3d_{5/2}$ (not shown) permits us to estimate the degree of substrate oxidation and interdiffusion at the interface during growth of the iron oxide. The main As $2p_{3/2}$ component at a binding energy of 1322.2 eV

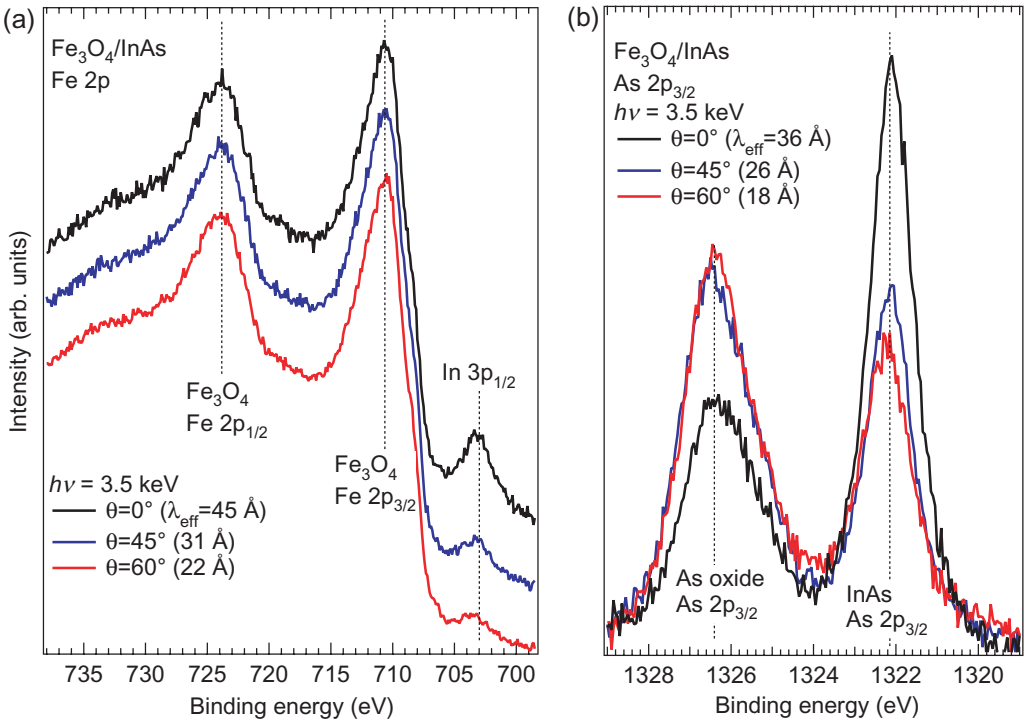

Figure 2. (a) Angle-resolved HAXPES spectra of the Fe 2p core-level in a Fe_3O_4/InAs thin film. The spectra are offset for better clarity. (b) Corresponding As $2p_{3/2}$ spectra, normalized to same integral spectral weight.

Table 1. Fe_3O_4/InAs: HAXPES spectral weight (given in per cent) for the various atomic species in sample 1 ($T_{growth} = 580$ K) and sample 2 ($T_{growth} = 650$ K). The probing depth decreases with the cosine of the emission angle, which is taken with respect to the surface normal.

Sample emission angle θ	No. 1		No. 2	
	0°	60°	0°	45°
In (overall)	3.3	1.2	8.8	8.2
As (InAs)	1.8	1.0	1.1	0.5
As (As_2O_3)	1.4	1.7	2.0	1.8
Fe (Fe_3O_4)	34.6	35.7	29.6	30.1
O (overall)	49.4	45.4	52.3	51.3
C (surf. cont.)	9.4	15.1	6.2	8.1

is readily assigned as intrinsic substrate signal, i.e. to In–As bonding. In contrast, a second component at higher binding energy (1326.4 eV) can clearly be attributed to the As oxides As_2O_3 and As_2O_5. This oxide fraction increases considerably with respect to the intrinsic InAs signal for larger electron emission angle θ, which implies smaller probing depth and thus higher interface sensitivity (see table 1). It should be emphasized here that such interface-sensitive depth profiling has only become possible due to the overall high photoelectron mean free path

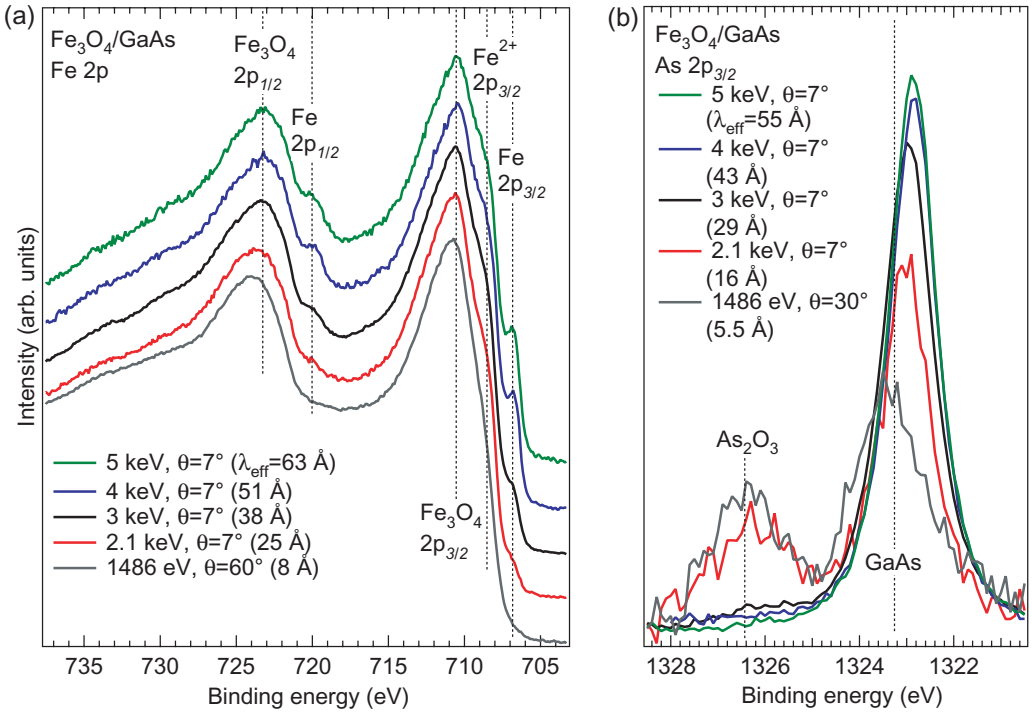

Figure 3. HAXPES Fe 2p (a) and As $2p_{3/2}$ (b) spectra of an Fe_3O_4/GaAs thin film for various photon energies. $\lambda_{eff} = \lambda \cos\theta$, where λ is the calculated inelastic mean free path of the photoelectron corresponding to its kinetic energy [28].

at the relevant HAXPES energies. No substrate signal was detectable in conventional XPS with Al–K_α radiation on the same sample.

The amount of As oxides did not vary significantly when changing the film growth temperature from 575 to 650 K. In contrast, the In $3d_{5/2}$ signal was considerably stronger at the same nominal Fe_3O_4 film thickness for the higher growth temperature, indicating pronounced In diffusion toward the sample surface (table 1). The chemical shift of the In $3d_{5/2}$ binding energy between InAs and In_2O_3 is at most 0.2 eV according to [27] and therefore cannot be resolved with our energy resolution.

3.3.2. Fe_3O_4/GaAs. The method of post-oxidation of an elemental Fe film was chosen for the GaAs substrate, since this procedure was successfully applied for the production of a magnetite thin film by Lu *et al* [20]. It is known from the literature that Fe grows epitaxially on GaAs [29] and that the growth mode depends on substrate temperature and reconstruction. The growth is e.g. 3D on Ga-rich GaAs(100)-c(8×2) with islands coalescing above four monolayers [30] or predominantly layer-by-layer on As-rich GaAs(100)-(2×4) [31]. This is in the first order due to the small lattice mismatch of 1.4% between Fe and GaAs. Therefore, it can be assumed that the initial Fe layer covers the substrate completely. In contrast the lattice mismatch between the designated Fe_3O_4 layer and GaAs is 5.0% and therefore considerably larger. LEED results on Fe_3O_4/GaAs indicate mono-crystalline growth of the initial Fe layer and the post-oxidized film.

Post-oxidation of the initial Fe layer results in a near-stoichiometric magnetite layer at the surface and a deeper-lying elemental Fe layer obviously localized at the interface, as inferred from the photon-energy-dependent HAXPES spectra in figure 3(a). Note that in these data

the HAXPES probing depth increases by nearly one order of magnitude from $h\nu = 1.486$ to 5 keV (see values for the inelastic mean free path in the figure). The overall Fe 2p spectrum is a superposition of the broad spin–orbit-split peaks at 710.5 and 724.0 eV with smaller and narrower peaks corresponding at 706.5 and 719.5 eV, which are characteristic of metallic Fe. From the spectra it is obvious that the spectral weight of the elemental Fe component is enhanced for increasing photon energy, i.e. for increasing probing depth and hence interface sensitivity. Moreover, the metallic Fe signal is suppressed in conventional and hence more surface-sensitive XPS spectra (measured with Al–K_α radiation). This behavior strongly suggests that an elemental Fe layer is situated right at the interface to GaAs.

Generally, the post-oxidation procedure is expected to introduce a vertically varying oxidation state profile in the film, resulting in a high oxidation state at the film surface and lower oxidation state toward the interface. This behavior can be attributed to the limited permeability of the Fe oxide layer for O_2 molecules. The film thickness, which can be produced via this method, is therefore restricted to only a few nanometers. However, higher film thicknesses beyond can, in principle, be attained with repeated Fe evaporation and post-oxidation cycles.

As $2p_{3/2}$ (see figure 3(b)) and Ga $2p_{3/2}$ (not shown) display considerably less oxide layer formation than observed in the Fe_3O_4/InAs system. A small As oxide component at 1325.6 eV is observed for small photon energy and hence probing depth, but strongly suppressed at much higher excitation energies. From these photon energy-dependent depth profiling data, we conclude that the small As and Ga oxide signal originates from the interface. The initially grown Fe layers act as barrier for the O_2 molecules and protect the substrate surface from unintentional oxidation deeper in the bulk. With decreasing probing depth (i.e. smaller photon energy) the intrinsic As $2p_{3/2}$ peak appears to shift to higher binding energy. This behavior is presently not yet understood and requires further investigation. One may speculate that it could be related to band bending at the interface, or reflect an increasing contribution by covalent Fe–As bonds in the more interface-sensitive spectra.

We thus find that depth profiling with HAXPES, either by varying the photoelectron escape angle or by tuning the photon energy, is a valuable tool for the characterization of oxide films on semiconductor substrates. The above HAXPES data provide helpful guidance for the optimization of the film growth parameters and, in particular, important information on composition and chemistry of the interface. The latter is essential for the efficiency of spin injection from the magnetite electrode into the semiconductor substrate. It will be interesting to correlate the spectroscopic findings with actual spin transport experiments. Another important aspect is the actual spin polarization in the magnetite film, and its possible vertical variation from surface to interface. This could, in principle, be determined by magnetic circular dichroism in HAXPES or by spin-resolved HAXPES. While the former has already been shown to be a feasible method [32], the latter requires the development of novel types of spin detectors with enhanced efficiency.

4. $LaAlO_3$/$SrTiO_3$ (LAO/STO) heterostructures

4.1. Motivation: Novel conducting interface phase between band insulators

The system LAO/STO is probably the most intensively studied oxide heterostructure since the first theoretical proposals [33] and experimental reports [34] that novel metallic interface phases can be induced in such systems, although the constituent materials are insulating. In the case

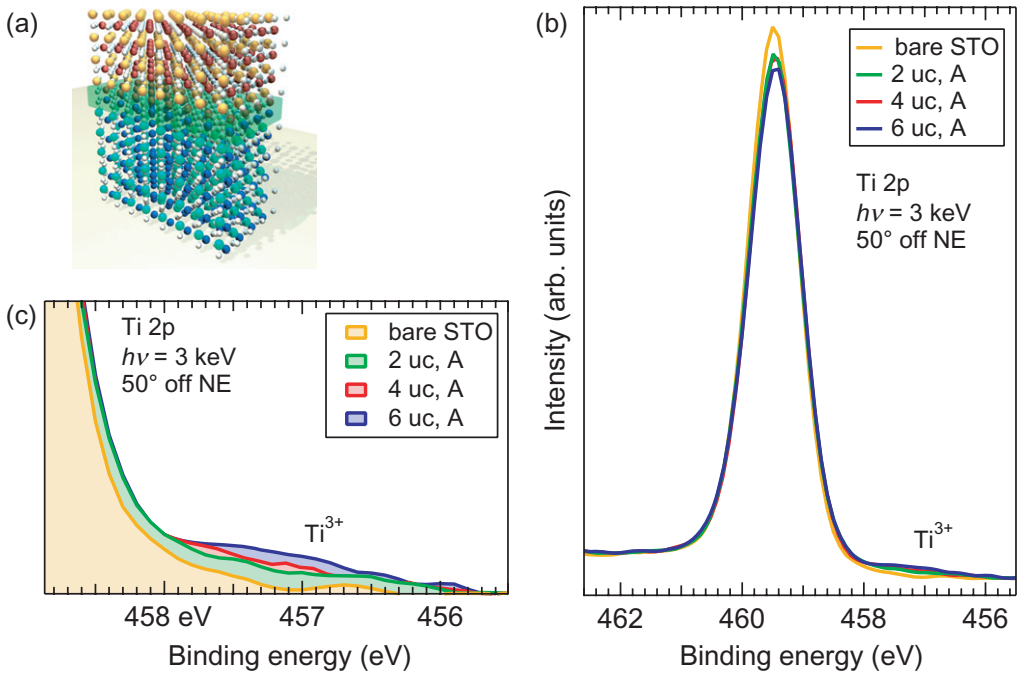

Figure 4. (a) Sketch of an LAO/STO heterostructure with a 2D interface electron gas. (b) Ti 2p spectra LAO/STO samples with various numbers of LAO overlayers and a bare STO substrate, measured at a fixed emission angle of 50° off normal emission (NE). The Ti^{3+} signal is a direct manifestation of additional electrons in the Ti 3d states and hence of the interface 2DEG. Samples from the University of Augsburg (A). (c) Close-up of the Ti^{3+} weight of the spectra in (b).

of LAO and STO, both compounds are wide-gap semiconductors with perovskite structure. An artistic view of an LAO/STO heterostructure with a 2D electron gas (2DEG) at the interface is shown in figure 4(a).

The 2DEG has a number of fascinating properties. First of all, it only exists in interfaces on TiO_2-terminated STO, while no metallic interface phase has been observed on SrO-terminated STO [34]. Also, the 2DEG only occurs, if the LAO overlayer equals or exceeds a critical thickness. Furthermore, the 2DEG can be controlled by field effect, i.e. by applying a gate voltage the interface can be driven from conducting to insulating or *vice versa* [35]. At low temperatures, many-body effects drive the 2DEG into a new symmetry-broken phase, although quite different types of groundstates have been observed: while some groups found 2D superconductivity below 200 mK, others reported on indications for ferromagnetism below 1 K [36]–[38].

Besides these highly interesting observations, the very reason for the formation of a 2DEG between the two band insulators LAO and STO is still an open question. Both extrinsic and intrinsic explanations have been put forward. For example, it has been found that a low oxygen partial pressure during PLD film growth results in oxygen vacancies, which act as donors and create n-type mobile charge carriers in the STO substrate [38]. Likewise, off-stoichiometry as a result of Sr/La mixing [39] can induce interface conductivity. On the other hand, conventional band-bending [40], accounting for the band discontinuity of the two materials, has been

suggested to trap electrons in a narrow region at the inner LAO/STO interface. However, none of these models is capable of explaining the threshold behavior with growing LAO overlayer thickness.

An alternative explanation for 2DEG formation, which takes into account the ionic character of the involved perovskites, has been at issue under the notion of 'electronic reconstruction'. In this picture, owing to the polar nature of the stacked LAO crystal planes, an electrostatic potential is piled up with increasing number of LAO overlayers [41]. A so-called polar catastrophe can be avoided by charge transfer from the LAO surface to the LAO/STO interface, in the simplest description by half an elementary charge per 2D unit mesh. The probably most striking experimental fact in support of this scenario is indeed the existence of a critical LAO thickness, which was first reported by Thiel *et al* [35] by transport and Hall measurements. They found that at an overlayer thickness of four LAO unit cells the conductivity jumps from a value below the measuring limit to a constant value, indicative of metallic coherent charge transport. This observation cannot easily be reconciled with any of the other above explanations. In the following, we will show how HAXPES can provide valuable information on two key quantities, namely the thickness and the charge density of the 2DEG [42]. Furthermore, we demonstrate the power of HAXPES in total reflection geometry, which allows depth profiling at considerably higher count rate than by conventional angle- or photon energy-dependent spectroscopy.

4.2. Results

Figure 4(b) displays Ti $2p_{3/2}$ core-level spectra at a fixed emission angle of 50° for samples from Augsburg with a varying number of LAO overlayers in comparison to a bare STO spectrum. The spectra are normalized to equal integral intensity. As can be seen, the peak maximum decreases with increasing number of LAO unit cells (uc). In contrast, at the foot of the peak at lower binding energies, there is a corresponding increase of spectral weight. This is better assessed from the close-up of this region in figure 4(c). The energy difference of 2.2 eV between the main peak and the weight occurring at its foot corresponds well to the chemical shift between Ti^{4+} and Ti^{3+}. This is further corroborated by the conservation of their total spectral weight, in agreement with a scenario in which more and more Ti atoms at or near the interface accept an extra electron, turning its valence from 4+ (as in pure STO) to 3+. Thus the ratio of the areas under the two lines is a measure for the 3d charge carrier concentration for a certain probing depth (determined by the emission angle and the chosen photon energy). From a quantitative analysis of these HAXPES spectra one can thus estimate absolute values for the interface charge density per unit area [42].

Despite the overall agreement with the results from transport regarding the size of the charge carrier density, there are two remarkable points to note: firstly, the increase in charge density is continuous, at variance with the transport data. Secondly, there is nonzero charge already for the 2 uc sample, again in contradiction to conductivity measurements in which it is found to be insulating. Probably several factors contribute to this seemingly contradictory results. There might be a certain amount of localized charge carriers at the STO interface, irrespective of the number of LAO overlayers. This amount is seen in HAXPES but does not contribute to conductivity. Partly, the absence of a sharply defined critical LAO thickness in the HAXPES data might be traced back to charge carriers which are photogenerated upon the irradiation with x-rays. Due to the large penetration depth such carriers are created deep in the

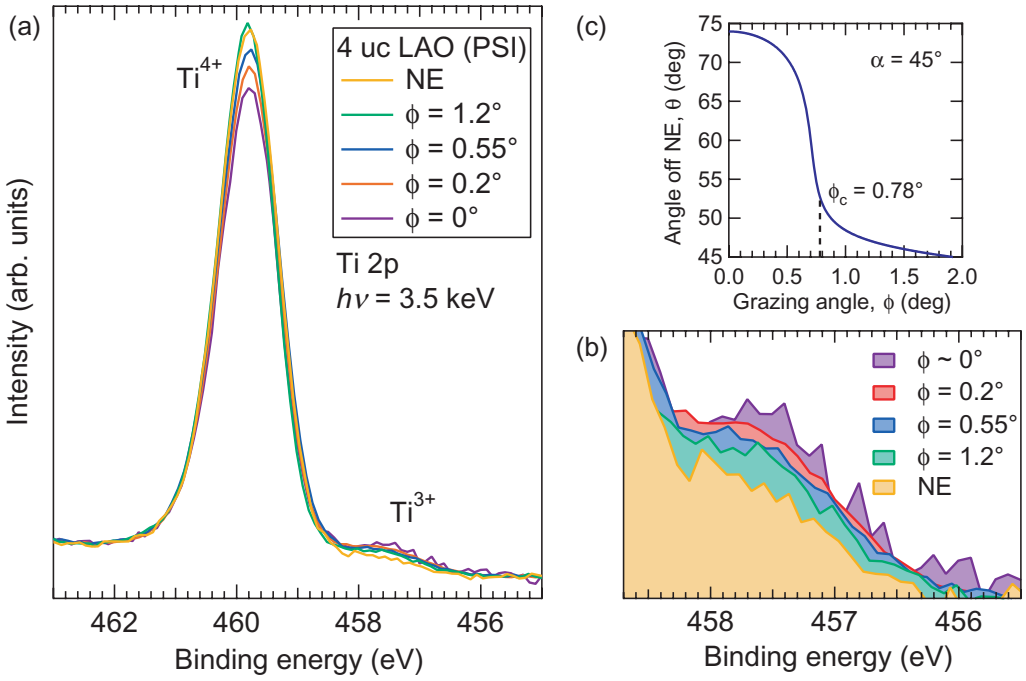

Figure 5. (a) Ti 2p spectra of a 4 uc sample for various grazing angles ϕ about the critical angle of total reflection ϕ_c. Sample from the Paul-Scherrer-Institute (PSI). (b) Close-up of the Ti^{3+} weight of the spectra in (a). (c) Relation between the grazing angle, ϕ, and the angle off normal emission (NE), θ, in a non-grazing emission geometry, corresponding to equal effective electron escape depths (calculated for $\alpha = 45°$). See figure 1 for definition of angles.

substrate. With increasing LAO thickness and hence increasing electrostatic potential gradually more and more of these carriers might be collected at the interface. Finally, our quantitative analysis [42] yields a 2DEG thickness of the order of 1 uc, in agreement with density-functional calculations [43]. For such a situation, substrate terraces might hinder electron conduction until a large enough density is reached.

As touched upon above, a quantitative analysis based on a simple model for the heterostructure is straightforward, if one uses the variation of the electron emission angle for depth profiling. It essentially involves only knowledge of the electron inelastic mean free path. An example for depth profiling by means of external total reflection in a grazing incidence geometry is given in figures 5(a) and (b). In these plots, Ti 2p core-level spectra and the corresponding close-ups of the Ti^{3+} related weight, respectively, on a 4 uc sample fabricated at the PSI are shown for various grazing angles around the critical angle for total external reflection. Qualitatively the same results are obtained as by the conventional depth profiling method, i.e. with increasing sensitivity to the interface (smaller ϕ) an increase of the relative Ti^{3+} weight is observed. However, a quantitative analysis is more intricate, since in addition to the mean electron scattering length also the optical constants of the material and the experimental geometry with respect to both electron emission and light incidence have to be taken into account. If these aspects are properly considered, one can calculate the functional relationship between the electron emission angle θ in standard depth profiling geometry and the grazing

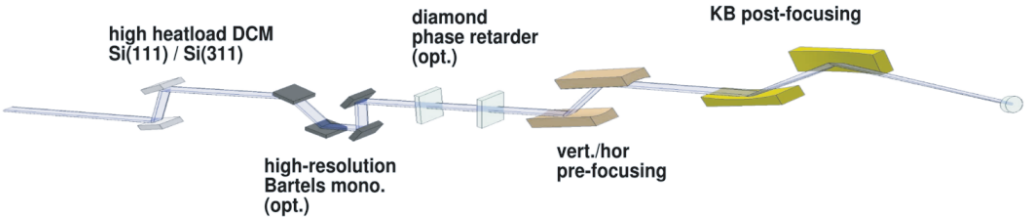

Figure 6. Schematic arrangement of the x-ray optical elements used for HAXPES at undulator beamline P09 of PETRA III.

angle ϕ for equal effective probing depths. This highly nonlinear curve is plotted in figure 5(c) for a fixed angle α between light incidence and electron emission (here $\alpha = 45°$). Note that, coming from larger angles, the critical angle ϕ_c marks the onset below which a change in ϕ most sensitively results in a variation of the effective probing depth.

5. Perspectives

Currently there are about 12 HAXPES instruments in operation at various synchrotron radiation facilities worldwide (see [5] for details). The technique has rapidly developed over the past few years, with widespread applications from basic research to applied materials science. In order to meet the growing demand and to meet special requirements, a number of new dedicated HAXPES set-ups are currently being planned or already under construction.

New perspectives for high-resolution HAXPES will arise at DESY with the availability of a dedicated station at PETRA III, which is designed to become the highest brilliance hard x-ray storage ring source worldwide. Source brilliance is one of the key ingredients for high-resolution hard x-ray spectroscopy on nano-sized materials. Not only does the brilliant beam allow for high-energy resolution with appreciable photon flux but also the small photon source size can be effectively utilized to reach μm focusing.

A new HAXPES instrument is currently being built as an endstation at beamline P09 of PETRA III. The photon source is a spectroscopy undulator covering an energy range of 2.4–10 keV in the first harmonic with high flux of the order of 10^{13} photons s^{-1} into a band width of $\Delta\nu/\nu = 10^{-4}$. The beamline comprises a number of x-ray optical elements (figure 6) facilitating a range of interesting options for HAXPES experiments. The energy resolution obtained from the primary Si(311) high heat-load monochromator is expected to be 100–200 meV in the range from 4.2 to 7 keV photon energy. Higher resolution well below 100 meV may be obtained by optionally using a Bartels-type post monochromator with interchangeable crystal sets. Due to the high source brilliance, the monochromator throughput will be large, resulting in a photon flux of typically $>10^{11}$ photons s^{-1} within a $\sim$40 meV energy bandpass.

Moderate focusing down to about 200 μm^2 is obtained by a pair of pre-focusing mirrors. For laterally resolving experiments on nanostructures by photon beam scanning, post-focusing by a Kirkpatrick–Baez (KB) mirror system close to the experiment will result in a focal spot of 1–5 μm^2 on the sample. It is noted that the HAXPES experiment is located 95 m from the source allowing for convenient focal distances. For studies on magnetic materials, a double-stage diamond phase retarder may be optionally placed into the monochromatic beam providing variable circular polarization for, e.g. core level XMCD experiments. Its usable energy range for

HAXPES is from about 4.5 to 10 keV with diamond plates of different thicknesses yielding an overall transmission of 30–40%. Note that by also using the second stage a half-wave plate condition is realized, which allows continuous rotation of the linear polarization as well.

The HAXPES instrument itself uses a SPECS Phoibos 225 electron analyzer reaching up to 15 keV kinetic energy with a design energy resolution well below 100 meV. Since the counting rates of valence band spectra may be low in HAXPES experiments, the instrument uses a delayline detector that can optionally be combined with a micro-Mott spin detector for photoelectron spin analysis. The samples can be precisely aligned with a motorized five-axis manipulator with integrated LHe-cryostat ($T < 18$ K).

This set-up is currently being tested and commissioned in parallel to the assembly of the PETRA III beamline. It is planned to perform initial HAXPES experiments in summer 2009. After commissioning, this new HAXPES instrument will provide interesting new opportunities for the study of bulk electronic properties of complex correlated and, in particular, magnetic materials, embedded interfaces and nanostructures, multifunctional composite materials as well as magnetic devices.

Acknowledgments

We are indebted to J Mannhart and S Thiel (both at University of Augsburg, Germany) and PR Willmott and CW Schneider (PSI, Switzerland) for providing high-quality LAO/STO samples. We also thank M Gorgoi, M Mertin, F Schäfers (all at BESSY) as well as H Schulz-Ritter and S Thiess (DESY) for their excellent assistance at the synchrotron experiments. Financial support of the BMBF (grant 05 KS7WW3), the Helmholtz-Centre Berlin for Materials and Energy (HZB), and DESY is gratefully acknowledged.

References

[1] Hüfner S 1995 *Photoelectron Spectroscopy* (Heidelberg: Springer)
[2] Hüfner S, Claessen R, Reinert F, Straub Th, Strocov V N and Steiner P 1999 *J. Electron Specrosc. Relat. Phenom.* **100** 191
[3] Reinert F and Hüfner S 2005 Photoemission spectroscopy—from early days to recent applications *New J. Phys.* **7** 97
[4] Kobayashi K *et al* 2003 *Appl. Phys. Lett.* **83** 1005
[5] Kobayashi K 2009 Hard x-ray photoemission spectroscopy *Nucl. Instrum. Methods Phys. Res.* A **601** 32
[6] Imada M, Fujimori A and Tokura Y 1998 *Rev. Mod. Phys.* **70** 1039
[7] Ramirez A P 2007 *Science* **315** 1377
[8] Schäfers F, Mertin M and Gorgoi M 2007 KMC-1: a high resolution and high flux soft x-ray beamline at BESSY *Rev. Sci. Instrum.* **78** 123102
[9] Drube W, Grehk T M, Treusch R and Materlik G 1998 Tunable high-energy x-ray photoemission *J. Electron Spectrosc. Relat. Phenom.* **88** 683
[10] Haghiri-Gosnet A M, Arnal T, Soulimane R, Koubaa M and Renard J P 2004 Spintronics: perspectives for the half-metallic oxides *Phys. Status Solidi* A **201** 1392–7
[11] Wolf S A, Awschalom D D, Buhrman R A, Daughton J M, von Molnar S, Roukes M L, Chtchelkanova A Y and Treger D M 2001 Spintronics: a spin-based electronics vision for the future *Science* **294** 1488–95
[12] Datta S and Das B 1990 Electronic analog of the electrooptic modulator *Appl. Phys. Lett.* **56** 665–7
[13] Yanase A and Hamada N 1999 Electronic structure in high temperature phase of Fe_3O_4 *J. Phys. Soc. Japan* **68** 1607–13

[14] Miles P A, Westphal W B and Von Hippel A 1957 Dielectric spectroscopy of ferromagnetic semiconductors *Rev. Mod. Phys.* **29** 279–307
[15] Schmidt G, Ferrand D, Molenkamp L W, Filip A T and van Wees B J 2000 Fundamental obstacle for electrical spin injection from a ferromagnetic metal into a diffusive semiconductor *Phys. Rev.* B **62** R4790–3
[16] Alvarado S F, Erbudak M and Munz P 1976 Final-state effects in 3d photoelectron-spectrum of Fe_3O_4 and comparison with Fe_xO *Phys. Rev.* B **14** 2740–5
[17] Morton S A, Waddill G D, Kim S, Schuller I K, Chambers S A and Tobin J G 2002 Spin-resolved photoelectron spectroscopy of Fe_3O_4 *Surf. Sci.* **513** L451–7
[18] Fonin M, Pentcheva R, Dedkov Y S, Sperlich M, Vyalikh D V, Scheffler M, Rudiger U and Guntherodt G 2005 Surface electronic structure of the Fe_3O_4(100): evidence of a half-metal to metal transition *Phys. Rev.* B **72** 104436
[19] Dedkov Y S, Rudiger U and Guntherodt G 2002 Evidence for the half-metallic ferromagnetic state of Fe_3O_4 by spin-resolved photoelectron spectroscopy *Phys. Rev.* B **65** 064417
[20] Lu Y X, Claydon J S, Xu Y B, Thompson S M, Wilson K and van der Laan G 2004 Epitaxial growth and magnetic properties of half-metallic Fe_3O_4 on GaAs(100) *Phys. Rev.* B **70** 233304
[21] Jain S, Adeyeye A O and Boothroyd C B 2005 Electronic properties of half metallic Fe_3O_4 films *J. Appl. Phys.* **97** 093713
[22] Ferhat M and Yoh K 2007 High quality $Fe_{3-\delta}O_4$/InAs hybrid structure for electrical spin injection *Appl. Phys. Lett.* **90** 112501
[23] Preisler E J, Brooke J, Oldham N C and McGill T C 2003 Pulsed laser deposition growth of Fe_3O_4 on III–V semiconductors for spin injection *J. Vac. Sci. Technol.* B **21** 1745–8
[24] Paul M, Müller, Ruff A, Schmid B, Berner G, Mertin M, Sing M and Claessen R 2009 Probing the interface of Fe_3O_4/GaAs thin films by hard x-ray photoelectron spectroscopy *Phys. Rev.* B **79** 233101
[25] Gota S, Moussy J B, Henriot M, Guittet M J and Gautier-Soyer M 2001 Atomic-oxygen-assisted mbe growth of Fe_3O_4 (111) on alpha-Al_2O_3 (0001) *Surf. Sci.* **482** 809–16
[26] Kim Y J, Gao Y and Chambers S A 1997 Selective growth and characterization of pure, epitaxial alpha-Fe_2O_3(0001) and Fe_3O_4(001) films by plasma-assisted molecular beam epitaxy *Surf. Sci.* **371** 358–70
[27] Hollinger G, Skheytakabbani R and Gendry M 1994 Oxides on GaAs and InAs surfaces—an x-ray-photoelectron-spectroscopy study of reference compounds and thin oxide layers *Phys. Rev.* B **49** 11159–67
[28] Tanuma S, Shiratori T, Kimura T, Goto K, Ichimura S and Powell C J 2005 Experimental determination of electron inelastic mean free paths in 13 elemental solids in the 50 to 5000 ev energy range by elastic-peak electron spectroscopy *Surf. Interface Anal.* **37** 833–45
[29] Xu Y B, Kernohan E T M, Freeland D J, Ercole A, Tselepi M and Bland J A C 1998 Evolution of the ferromagnetic phase of ultrathin Fe films grown on GaAs(100)-4 × 6 *Phys. Rev.* B **58** 890–6
[30] Chambers S A, Xu F, Chen H W, Vitomirov I M, Anderson S B and Weaver J H 1986 Simultaneous epitaxy and substrate out-diffusion at a metal–semiconductor interface—Fe/GaAs(001)-C(8 × 2) *Phys. Rev.* B **34** 6605–11
[31] Kneedler E, Thibado P M, Jonker B T, Bennett B R, Whitman L J, Shanabrook B V and Krebs J J 1996 Fe adsorption and film growth on GaAs(001) (2 × 4)-As *J. Appl. Phys.* **79** 5125
[32] Ueda S, Tanaka H, Takaobushi J, Ikenaga E, Kim J-J, Kombata M, Kawai T, Osawa H, Kawamura N, Suzuki M and Kobayashi K 2008 Hard x-ray photoemission spectroscopy combined with magnetic circular dichroism: application to $Fe_{3-x}Zn_xO_4$ spinel oxide thin films *Appl. Phys. Express* **1** 077003
[33] Okamoto S and Millis A J 2004 Electronic reconstruction at an interface between a Mott insulator and a band insulator *Nature* **428** 630
[34] Ohtomo A and Hwang H Y 2004 A high-mobility electron gas at the $LaAlO_3/SrTiO_3$ heterointerface *Nature* **427** 423
[35] Thiel S, Hammerl G, Schmehl A, Schneider C W and Mannhart J 2006 Tunable quasi-two-dimensional electron gases in oxide heterostructures *Science* **313** 1942
[36] Reyren N *et al* 2007 Superconducting interfaces between insulating oxides *Science* **317** 1196

[37] Caviglia A D, Gariglio S, Reyren N, Jaccard D, Schneider T, Gabay M, Thiel S, Hammerl G, Mannhart J and Triscone J-M 2008 *Nature* **456** 624

[38] Brinkman A, Huijben M, van Zalk M, Huijben J, Zeitler U, Maan J C, van der Wiel W G, Rijnders G, Blank D H A and Hilgenkamp H 2007 Magnetic effects at the interface between non-magnetic oxides *Nat. Mater.* **6** 493

[39] Willmott P R *et al* 2007 Structural basis for the conducting interface between $LaAlO_3$ and $SrTiO_3$ *Phys. Rev. Lett.* **99** 155502

[40] Yoshimatsu K, Yasuhara R, Kumigashira H and Oshima M 2008 Origin of metallic states at the heterointerface between the band insulators $LaAlO_3$ and $SrTiO_3$ *Phys. Rev. Lett.* **101** 026802

[41] Nakagawa N, Hwang H Y and Müller D A 2006 Why some interfaces cannot be sharp *Nat. Mater.* **5** 204

[42] Sing M *et al* 2009 Profiling the interface electron gas of $LaAlO_3/SrTiO_3$ heterostructures with hard x-ray photoelectron spectroscopy *Phys. Rev. Lett.* **102** 176805

[43] Janicka K, Velev J P and Tsymbal E Y 2009 Quantum nature of two-dimensional electron gas confinement at $LaAlO_3/SrTiO_3$ interfaces *Phys. Rev. Lett.* **102** 106803